Proceedings of the
International Conference on Mechanical Engineering 2005
(ICME2005) 28- 30 December 2005, Dhaka, Bangladesh

ICME05-TH-16

ANALYSIS OF A MATRIX HEAT EXCHANGER OF CIRCULAR GEOMETRY

F. Farhani[1] and S. Sarangi[2]

[1]Mechanical Engineering Department, I.R.O.S.T., P.O. Box 15815–3538, Tehran, Iran,
[2]Cryogenic Engineering Centre, I.I.T., Kharagpur–721302, India.

ABSTRACT

The standard heat exchanger relations can not be directly applied to matrix heat exchangers, due to factors such as discontinuous temperature profile along the exchanger length, variation of plate and fluid temperatures in both axial and radial directions, the heterogeneous wall and the finite number of plates. Therefore, to predict the performance of these exchangers under given operating conditions, the set of governing equations has to be integrated and solved simultaneously. In this paper a numerical procedure has been used to analyze a matrix heat exchanger of circular geometry. The governing equations have been derived in the cylindrical coordinate system and the resulting set of partial differential equations has been simplified, using well justified assumptions. The partial differential equations are reduced to a set of algebraic and ordinary differential equations which are then solved using a standard iterative algorithm. Using a computer program, the steady state performance of the perforated-plate heat exchanger of circular geometry has been predicted. The results of the present work have been compared with those of other researchers.

Keywords: Matrix Heat Exchanger, Circular Geometry, Governing Equations, Steady State Performance

1. INTRODUCTION

A *matrix heat exchanger* (MHE), shown in Fig. 1, consists of a set of perforated-plates (copper or aluminum), stacked alternately with an equal number of spacers (plastics, stainless steel). It is used in low power cryocoolers and helium liquefiers.

In an MHE, due to the thin (l< 1.0 mm), conducting plates, the Biot number is less than 0.1 in the axial direction [1]. Hence, a plate is assumed to be at a uniform temperature over its thickness, which has been experimentally confirmed by Kirpikov and Leifman [2].

The plates of an MHE are often considered as fins [1]. However, due to non-uniform fluid temperature, the standard fin formula is not adequate. In addition, standard heat exchanger relations can not be applied to an MHE directly. Therefore, for prediction of performance of an MHE, the set of governing equations must be integrated and solved simultaneously.

Venkatarathnam [3] analyzed an MHE of rectangular cross section. Farhani [4] extended his work to include MHEs of circular cross section. The non-uniform flow channel widths add to the complexity of the analysis.

In this paper, an MHE of circular geometry has been analyzed numerically. Using a computer program, the steady state performance of the heat exchanger has been predicted. The results of the present work have been compared with those of other researchers.

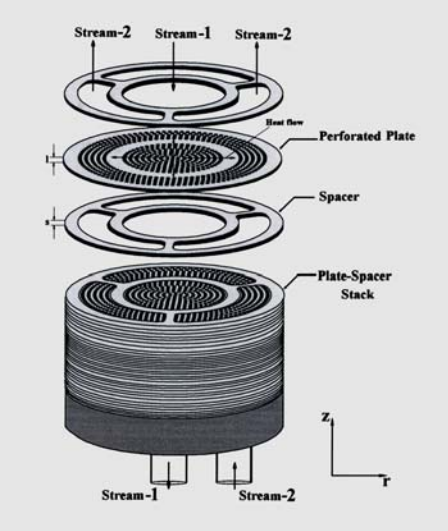

Fig 1. A circular matrix heat exchanger (MHE)

2. THE MATHEMATICAL MODEL

An MHE (Fig. 1) of total length L, consisting of n plates of thickness l, separated by spacers of thickness s is considered. The characteristic dimension of perforations is d. The heat transfer direction r is radial, while the fluid direction Z is axial. In Fig. 2, the warm stream (stream-1) with circular cross section of radius

R_1, flows through channel-1, while the cold stream (stream-2) with an annular cross section of radii R_s and R_2, Flows through channel-2. The two channels are separated by a wall of radial width $b\,(=R_s - R_1)$. Positive Z direction is the direction of flow of stream-1, and positive r direction is from channel-1 to channel-2.

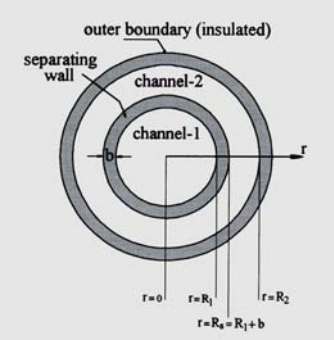

Fig 2. Spacer geometry, showing the relevant radii

The temperature of a plate in channel i is $T_{i,j(r)}$. The fluid in channel-1 enters the jth plate at $t_{1,j}(r)$ and leaves it at $t_{1,j+1}(r)$. Similarly, the fluid in channel-2 enters the jth plate at $t_{2,j+1}(r)$ and leaves it at $t_{2,j}(r)$. The fluid temperature inside a plate is $t(r,z)$.

2.1 Assumptions

(a) The plates are isothermal in axial direction (z),
(b) Wall temperature profile is linear with radius,
(c) Outermost surface is an insulating boundary.

2.2 Governing Equations

Performing an energy balance over a differential control volume in the plate (Fig. 3) and using Table 1:

$$\theta_{1,j+1} = \tau_{1,j} + \exp(-N_{tu,f,1})\,(\theta_{1,j} - \tau_{1,j}) \tag{1a}$$

$$\theta_{2,j} = \tau_{2,j} + \exp(-N_{tu,f,2})\,(\theta_{2,j+1} - \tau_{2,j}) \tag{1b}$$

$$\frac{d^2\tau_{1,j}}{d\eta_1^{\,2}} + 1/\eta_1 \frac{d\tau_{1,j}}{d\eta_1} = \frac{\left[1-\exp(-N_{tu,f,1})\right]}{\phi_1 N_{tu,f,1}}\left(\tau_{1,j} - \theta_{1,j}\right) \tag{2a}$$

$$\frac{d^2\tau_{2,j}}{d\eta_2^{\,2}} + \frac{1}{\eta_2+\zeta}\frac{d\tau_{2,j}}{d\eta_2} = \frac{\left[1-\exp(-N_{tu,f,2})\right]}{\phi_2 N_{tu,f,2}}\left(\tau_{2,j} - \theta_{2,j+1}\right) \tag{2b}$$

Where,
h = convective heat transfer coefficient,
A''' = heat transfer area per unit volume of the plate,
G = fluid mass velocity in the header,
C_p = fluid specific heat at constant pressure,
F = a constant, (+1) for stream-1 and (-1) for stream-2,
and $N_{tu,f,i} = \left(hA''' / GC_p\right)$, is N_{tu} of one side of a plate.

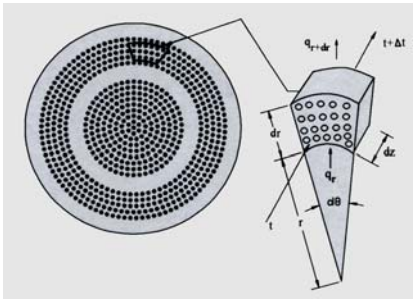

Fig 3. The differential control volume $rd\theta\ dr\ dz$

Table 1: Non-dimensional variables and parameters

$\theta = \dfrac{t - t_{2,in}}{t_{1,in} - t_{2,in}}$	$\eta_i = \dfrac{r_i}{\Delta_i}$
$\tau = \dfrac{T - t_{2,in}}{t_{1,in} - t_{2,in}}$	$N_{tu,p,i} = \dfrac{k_p l}{\left(GC_p\Delta^2\right)_i}$
$\phi_i = \dfrac{N_{tu,p,i}}{N_{tu,f,i}}$	$\zeta = \dfrac{R_s}{R_2 - R_s}$

Equations (1a) and (1b) form two sets of n algebraic equations in $\theta_{i,j}$ ($(2 \le j \le n+1)$ for stream-1, and $(1 \le j \le n)$ for stream-2), at any value of the radial coordinate η. The recurrence relation is:

$$\theta_{1,1} = 1 \quad \text{and} \qquad \theta_{2,n+1} = 0 \tag{3}$$

Equations (2a) and (2b) are two sets of second-order ordinary differential equations in $\tau_{i,j}$ (j=1, n and i=1, 2). The boundary conditions in dimensionless form are:

$$\left(\frac{d\tau_{1,j}}{d\eta_1}\right)_{\eta_1=0} = 0 \tag{4a}$$

$$\left(\frac{d\tau_{2,j}}{d\eta_2}\right)_{\eta_2=1} = 0 \tag{4b}$$

The rate of heat transfer between the two streams through the ith plate is:

$$q_{i,j} = -k_p\left(A_r\right)_i \frac{dT_{i,j}}{dr} \tag{5}$$

where $A_r = 2\pi R_s l$ is the radial heat flow area in

channel-2, and $\frac{dT_{i,j}}{dr}$ is computed at $r = R_1$ for channel-1, and at $r = R_s$ for channel-2 (see Fig. 3). For the individual channels, Eq. (5) becomes:

$$q_{1,j} = -k_p(2\pi\ R_1 l)\left(\frac{dT_{1,j}}{dr}\right)_{r=R_1} \tag{6a}$$

$$q_{2,j} = -k_p(2\pi\ R_s l)\left(\frac{dT_{2,j}}{dr}\right)_{r=R_s} \tag{6b}$$

Let us define a dimensionless heat flow rate $\chi_{i,j}$ as:

$$\chi_{i,j} = \frac{q_{i,j}}{(A_c GC_p)_i (t_{1,in} - t_{2,in})} \tag{7}$$

$(A_c)_i = \pi\ R_1{}^2$ (channel-1), $\pi\left(R_2{}^2 - R_s{}^2\right)$(channel-2) is the free flow area of the *i*th channel.

Using Eq. (7), Eq. (5) is reduced to the following:

$$\chi_{i,j} = -\sigma_i\ N_{tu,p,i}\frac{d\tau_{i,j}}{d\eta_i} = -\sigma_i\ \phi_i\ N_{tu,f,i}\frac{d\tau_{i,j}}{d\eta_i} \tag{8}$$

where $\frac{d\tau_{i,j}}{d\eta_i}$ is computed at $\eta_1 = 1$ and $\eta_2 = 0$. σ_i is equal to 2 (channel-1), and $2R_s/R_2 + R_s$ (channel-2).

Defining boundary temperatures $T_{1s,j} = (T_{1,j})_{r=R_1}$ and $T_{2s,j} = (T_{2,j})_{r=R_s}$, and expressing them in dimensionless form we have:

$$\tau_{1s,j} = (\tau_{1,j})_{\eta_1=1} \tag{9a}$$

$$\tau_{2s,j} = (\tau_{2,j})_{\eta_2=0} \tag{9b}$$

2.3 Heat Transfer in the Separating Wall

The Fourier conduction equation in cylindrical coordinates is applicable to the uniform wall separating the two channels:

$$k_{s,r}\left(\frac{\partial^2 T_s}{\partial r^2} + \frac{1}{r}\frac{\partial T_s}{\partial r}\right) + k_{s,z}\frac{\partial^2 T_s}{\partial z^2} = 0 \tag{10}$$

The effective mean thermal conductivities in axial and radial directions are [5]:

$$k_{s,r} = \frac{lk_p + sk_s}{s+l} \qquad ; k_{s,z} = \frac{s+l}{l/k_p + s/k_s} \tag{11}$$

Physically, the plates are nearly isothermal in axial direction, while the spacers sustain a temperature gradient. Equation (10), on the other hand, predicts finite temperature change over both the elements. Therefore, we used an alternative approach, which makes the solution substantially simpler, while enhancing the overall accuracy [3, 4]. The following assumption is made in addition to earlier ones:

(d) The average of temperatures on both edges of the plate is taken as the temperature of the separator at the corresponding face.

Figure 4a, shows the longitudinal section of an MHE. Figure 4b shows a control volume and Fig. 4c shows the temperature profile.

The average heat flux through the wall is given as:

$$q_{1,j} + q_{2,j} = \frac{2\pi\ k_p l(R_s + R_1)}{R_s - R_1}(T_{1s,j} - T_{2s,j}) \tag{12}$$

An energy balance over the separator portion of the *j*th plate (Fig.4b) gives:

$$q_{1,j} - q_{2,j} = q_{s,j+1} - q_{s,j} \tag{13}$$

$$q_{s,j} = \pi\left(R_s{}^2 - R_1{}^2\right)\ \ k_s\frac{(T_{s,j-1} - T_{s,j})}{s} \tag{14a}$$

where $q_{s,j}$ is the heat flow rate into the separator portion of the *j*th plate from *(j-1)*th plate. Using assumption (d), we have $T_{s,j} = \frac{T_{1s,j} + T_{2s,j}}{2}$. The two ends of the exchanger are insulated:

$$q_{s,1} = 0 \qquad and \qquad q_{s,n+1} \tag{14b}$$

Substitutions in Eq. (13) give separator governing equations as:

$$\chi_{1,j} - \frac{\chi_{2,j}}{\nu} = \lambda_s\left(2\tau_{s,j} - \tau_{s,j+1} - \tau_{s,j-1}\right) \qquad for \quad (2 \le j \le n-1) \tag{15a}$$

$$\chi_{1,1} - \frac{\chi_{2,1}}{\nu} = \lambda_s\left(\tau_{s,1} - \tau_{s,2}\right) \tag{15b}$$

$$\chi_{1,n} - \frac{\chi_{2,n}}{\nu} = \lambda_s\left(\tau_{s,n} - \tau_{s,n-1}\right) \tag{15c}$$

Equation (12) is expressed in dimensionless form as:

$$\chi_{1,j} + \frac{\chi_{2,j}}{\nu} = 2\lambda_p\left(\tau_{1s,j} - \tau_{2s,j}\right) \tag{16}$$

ν is the capacity ratio, and λ_p and λ_s are the separator lateral and axial conduction parameters, respectively. Ψ is a dimensionless geometrical parameters. $\lambda_s = n\lambda$, where λ is the overall axial conduction parameter and *n* is the number of plate-spacer pairs [6, 7].

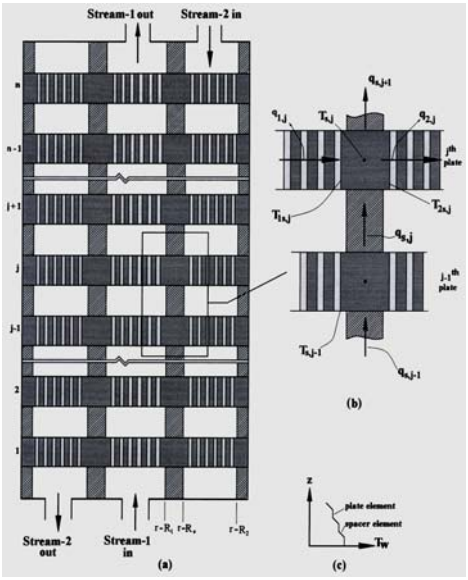

Fig 4. (a) Longitudinal section of an MHE, (b) Control volume, (c) Temperature profile in the exchanger

3. SOLUTION OF GOVERNING EQUATIONS

3.1 Simulation of Channel-1

Figure 5, shows the *j*th plate grid pattern and control volume. k=0 and k=m+1 are fictitious nodes.

Equations. (1a) and (2a) can now be written as:

$$\theta_{1,j+1,k} = \tau_{1,j,k} + A_1\,(\theta_{1,j,k} - \tau_{1,j,k})\,(0 \le k \le m+1) \quad (17)$$

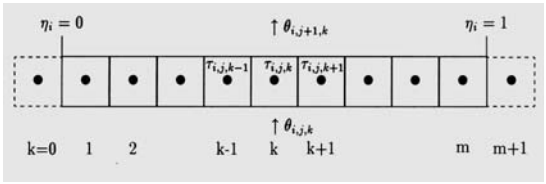

Fig. 5.Grid pattern and control volume for the *j*th plate

with $\theta_{1,1,k} = 1$, and

$$\frac{\tau_{1,j,k-1} - 2\tau_{1,j,k} + \tau_{1,j,k+1}}{\Delta\eta_1^{\,2}} + \frac{1}{(k-1/2)\Delta\eta_1}\left(\frac{\tau_{1,j,k+1} - \tau_{1,j,k-1}}{2\Delta\eta_1}\right) = \frac{(1-A_1)}{\phi_1 N_{tu,f,1}}\left(\tau_{1,j,k} - \theta_{1,j,k}\right)$$

where $A_1 = \exp\left(-N_{tu,f,1}\right)$. Further simplification gives:

$$\gamma_1\tau_{1,j,k-1} + B_1\tau_{1,j,k} + \gamma_2\tau_{1,j,k+1} = C_1\theta_{1,j,k}; \quad (1 \le k \le m-1) \quad (18)$$

where,

$$\eta_1 = \left(\frac{2k-2}{2k-1}\right); \eta_2 = \left(\frac{2k}{2k-1}\right); B_1 = C_1 - 2; \quad C_1 = \frac{(A_1-1)}{D_1}\Delta\eta_1 \;\; ; \; D_1 = \frac{\phi_1 N_{tu,f,1}}{\Delta\eta_1} \quad (19)$$

Boundary Eqs. (4a) and (9a) in Finite difference are:

$$\tau_{1,j,0} = \tau_{1,j,1} \quad (20a)$$

$$\tau_{j,m+1} = 2\tau_{1s,j} - \tau_{j,m} \quad (20b)$$

Equation (18) for nodes *k*=1 and *k*=m is modified as:

$$B_1\tau_{1,j,k} + \gamma_1\tau_{1,j,k+1} = C_1\theta_{1,j,k} \quad for \quad k = 1 \quad (21a)$$

and

$$\gamma_1\tau_{1,j,k-1} + (B_1 - \gamma_2)\tau_{1,j,k} = C_1\theta_{1,j,k} - 2\gamma_2\tau_{1s,j} \quad for \quad k = m \quad (21b)$$

Equations (18), (21a) and (21b) are combined and expressed in matrix notation as:

$$\begin{pmatrix} B_1 & \gamma_2 & & & \\ \gamma_1 & B_1 & \gamma_2 & & \\ & \ddots & \ddots & \ddots & \\ & & \ddots & \ddots & \\ & & & \gamma_1 & (B_1-\gamma_2) \end{pmatrix} \begin{pmatrix} \tau_{1,j,1} \\ \tau_{1,j,2} \\ \vdots \\ \vdots \\ \tau_{1,j,m} \end{pmatrix} = \begin{pmatrix} C_1\theta_{1,j,1} \\ C_1\theta_{1,j,2} \\ \vdots \\ \vdots \\ C_1\theta_{1,j,m} - 2\gamma_2\tau_{1s,j} \end{pmatrix} \quad (22)$$

The coefficient matrix in Eq. (22) is tridiagonal and can be inverted using the standard Thomas algorithm [8].

The dimensionless heat flux in channel-1-separating wall interface is determined from Eq. (8) as:

$$\chi_{1,j} = -2\phi_1 N_{tu,f,1}\left(\frac{\tau_{1,j,m+1} - \tau_{1,j,m}}{\Delta\eta_1}\right) \quad (23)$$

Substituting Eq. (20b) in Eq. (22) we get:

$$\chi_{1,j} = 4D_1\left(\tau_{1,j,m} - \tau_{1s,j}\right) \quad (24)$$

Equations (17) and (22) are the governing equations, and their solution yields temperature profile in a single (*j*th) plate. $\theta_{1,1,k}\ (1 \le k \le m)$ is known, hence, Eq. (22) is solved first, yielding $\tau_{1,1,k}\ (1 \le k \le m)$. These are then, used in Eq. (17) to calculate the $\theta_{1,2,k}\ (1 \le k \le m+1)$. The process is repeated for all plates, to find the entire temperature field in channel-1. The heat fluxes in the plate-separating wall boundary are calculated using Eq. (24).

3.2 Simulation of the Separating Wall

The sets of Eqs. (15a), (15b), (15c) and (16) form the governing equations of the separating wall, which can be solved for $\tau_{2s,j}$ and $\chi_{2,j}$ for $0 \le j \le n$, with specified

$\tau_{1s,j}$ and $\chi_{1,j}$, or vise versa. Substituting $\tau_{s,j} = \dfrac{\tau_{1s,j} + \tau_{2s,j}}{2}$ in Eqs. (15a), (15b), (15c) and eliminating $\tau_{2s,j}$ from these equations and Eq. (16):

$$\chi_{2,j-1} + A_s \chi_{2,j+1} = B_{s,j};\ 2 \le j \le n-1 \tag{25a}$$

$$(1 + A_s)\chi_{2,1} + \chi_{2,1} + \chi_{2,2} = B_{s,1} \tag{25b}$$

$$\chi_{2,n-1} + (1 + A_s)\chi_{2,n} = B_{s,n} \tag{25c}$$

where,

$$A_s = 4\frac{\lambda_p}{\lambda_s} - 2$$

$$B_{s,1} = -4\nu\lambda_p(\tau_{1s,1} - \tau_{1s,2}) + \nu\,(1 + 4\frac{\lambda_p}{\lambda_s})\,\chi_{1,1} - \nu\ \chi_{1,2}$$

$$B_{s,j} = -4\nu\lambda_p(2\tau_{1s,j} - \tau_{1s,j+1}\tau_{1s,j-1}) + \nu\,(2 + 4\frac{\lambda_p}{\lambda_s})\ \chi_{1,j} - \nu\ \chi_{1,j+1} - \nu\ \chi_{1,j-1} \quad (2 \le j \le n-1)$$

$$B_{s,n} = -4\nu\lambda_p(\tau_{1s,n} - \tau_{1s,n-1}) + \nu(1 + 4\frac{\lambda_p}{\lambda_s})\chi_{1,n} - \nu\,\chi_{1,n-1}$$

Equations (25a), (25b) and (25c) in matrix form are:

$$\begin{pmatrix} (A_s+1) & 1 & & & \\ 1 & A_s & 1 & & \\ & \cdot & \cdot & \cdot & \\ & & \cdot & \cdot & \\ & & & 1 & (A_s+1) \end{pmatrix} \begin{pmatrix} \chi_{2,1} \\ \chi_{2,2} \\ \cdot \\ \cdot \\ \chi_{2,n} \end{pmatrix} = \begin{pmatrix} B_{s,n} \\ B_{s,2} \\ \cdot \\ \cdot \\ B_{s,n} \end{pmatrix} \tag{26}$$

The coefficient matrix is tridiagonal and the equation can be solved for $\chi_{2,j}$, using Thomas algorithm [8].

3.3 Simulation of Channel-2

Equations (1b) and (2b) and boundary conditions (4b) and (9b), describe the fluid and plate temperature field in channel-2. The grid pattern for a plate is shown in shown in Fig. 5. Equations (1b) and (2b) can be written in finite difference form as:

$$\theta_{2,j,k} = \tau_{2,j,k} + A_2(\theta_{2,j+1,k} - \tau_{2,j,k})\ \ (0 \le k \le m+1) \tag{27}$$

with $\theta_{2,n+1,k} = 0$, and

$$\left(\frac{(k-1)+\dfrac{\zeta}{\Delta\eta_2}}{(k-1/2)+\dfrac{\zeta}{\Delta\eta_2}}\right)\tau_{2,j,k-1} + B_2\tau_{2,j,k} + \left(\frac{k+\dfrac{\zeta}{\Delta\eta_2}}{(k-1/2)+\dfrac{\zeta}{\Delta\eta_2}}\right)\tau_{2,j,k+1} = C_2\theta_{2,j+1,k} \tag{28}$$

where $A_2 = \exp(N_{tu,f,2})$, and $\zeta = \dfrac{R_s}{R_2 - R_s}$. For interior nodes, Eq. (28) is simplified as:

$$\left(\frac{k+\alpha-1}{k+\alpha-1/2}\right)\tau_{2,j,k-1} + B_2\tau_{2,j,k} + \left(\frac{k+\alpha}{k+\alpha-1/2}\right)\tau_{2,j,k+1} = C_2\theta_{2,j+1,k} \quad for\ 1 \le k \le m \tag{29}$$

where,

$$\alpha = \frac{\zeta}{\Delta\eta_2};\qquad D_2 = \frac{\phi_1 N_{tu,f,2}}{\Delta\eta_1};$$
$$C_2 = \frac{(A_2 - 1)}{D_2}\Delta\eta_2;\quad B_2 = C_2 - 2 \tag{30}$$

The boundary conditions for channel-2 are:

$$\tau_{2,j,m+1} = \tau_{2,j,m} \tag{31a}$$

$$\chi_{2,j} = \sigma_2 D_2(\tau_{2,j,0} - \tau_{2,j,1}) \tag{31b}$$

where $\sigma_2 = \dfrac{2R_s}{R_2 + R_s}$. Substituting Eqs. (31a) and (31b) in Eq. (29), we the boundary nodes:

Node $k = 1$:

$$\left(B_2 + \frac{2\alpha}{1+2\alpha}\right)\tau_{2,j,k} + \left[\frac{2(1+\alpha)}{1+2\alpha}\right]\tau_{2,j,k+1} = C_2\theta_{2,j+1,k} - \left(\frac{2\alpha}{1+2\alpha}\right)\frac{\chi_{2,j}}{\sigma_2 D_2} \tag{32a}$$

Node $k = m$:

$$\left(\frac{k+\alpha-1}{k+\alpha-1/2}\right)\tau_{2,j,k-1} + \left[B_2 + \left(\frac{k+\alpha}{k+\alpha-1/2}\right)\right]\tau_{2,j,k} = C_2\theta_{2,j+1,k} \tag{32b}$$

Defining:

$$\rho_1 = \left(\frac{2\alpha}{1+2\alpha}\right);\ \rho_2 = \left[\frac{2(1+\alpha)}{1+2\alpha}\right];$$
$$\rho_3 = \left(\frac{k+\alpha-1}{k+\alpha-1/2}\right);\ \rho_4 = \left(\frac{k+\alpha}{k+\alpha-1/2}\right),$$

and expressing Eq. (29), (32a) and (32b) in matrix form we get:

$$\begin{pmatrix} (B_2+\rho_1) & \rho_2 & & & \\ \rho_3 & B_2 & \rho_4 & & \\ & . & . & . & \\ & & . & . & \\ & & & \rho_3 & (B_2+\rho_4) \end{pmatrix} \begin{pmatrix} \tau_{2,j,1} \\ \tau_{2,j,2} \\ . \\ . \\ \tau_{2,j,m} \end{pmatrix}$$

$$= \begin{pmatrix} C_2\theta_{2,j+1,1} - \rho_1 \dfrac{\chi_{2,j}}{\sigma_2 D_2} \\ C_2\theta_{2,j+1,2} \\ . \\ . \\ C_2\theta_{2,j+1,m} \end{pmatrix} \qquad (33)$$

The coefficient matrix in Eq. (33) is tridiagonal, and the equation set is solved using Thomas algorithm [8].

Equations (27) and (33) are now the finite difference governing equations for channel-2. Since the fluid temperature $\theta_{2,n+1,k}$ ($1 \le k \le m$) for the nth plate is known, Eq. (33) for plate n is solved first, giving $\tau_{2,n,k}$ ($1 \le k \le m$). These results are then, used in Eq. (27) to calculate $\theta_{2,n,k}$ ($0 \le k \le m+1$). The process is repeated for all plates. Then, the dimensionless temperatures at the plate-separator interface are calculated as:

$$\tau_{2s,j} = \tau_{2,j,1} + \frac{\chi_{2,j}}{2\sigma D_2} \qquad (34)$$

3.4. The Solution Algorithm

An algorithm, similar to the one adopted by Venkatarathnam [3] has been used for simulation of a matrix heat exchanger of circular geometry, incorporating the analytical concepts and the finite difference schemes proposed earlier.

4. RESULTS AND DISCUSSION

A computer program was developed to predict the performance of an MHE of circular geometry.

The effective- N_{tu} (= $N_{tu,eff}$) is given as [6]:

$$N_{tu,eff} = \left(\frac{1}{1-\nu}\right) \ln\left(\frac{1-\nu\varepsilon}{1-\nu}\right) \qquad (35a)$$

which for a balanced flow operation ($\nu = 1$) becomes:

$$N_{tu,eff} = \frac{\varepsilon}{1-\varepsilon} \qquad (35b)$$

The design- N_{tu} (= $N_{tu,d}$) is given by the relation:

$$N_{tu,d} = \left[\frac{1}{N_{tu,f,1}} + \frac{1}{N_{tu,f,2}} + \frac{1}{\lambda_p}\right]^{-1} \qquad (36)$$

The inputs to this program are $N_{tu,f,1}$, $N_{tu,f,2}$, ϕ_1, ϕ_2, ν, λ_s, λ_p and n. To compare our results with those of other workers under similar conditions, we defined an overall conduction parameter, $\phi = \dfrac{A_{c1}\phi_1 + A_{c2}\phi_2}{A_{c1} + A_{c2}}$, which is a weighted average of the two ϕ values. Calculations were performed for $n = 50$ and $n = 100$, and for ϕ, ranging from 0.5 to 2.0. The range of $N_{tu,d}$ was $10 \le N_{tu,d} \le 1000$. The exchanger effectiveness has been computed as a function of geometrical and process parameters, and compared with solutions of Sarangi-Barclay [6], Kroeger [7], and Fleming [10] (see Figs. 6 through 11).

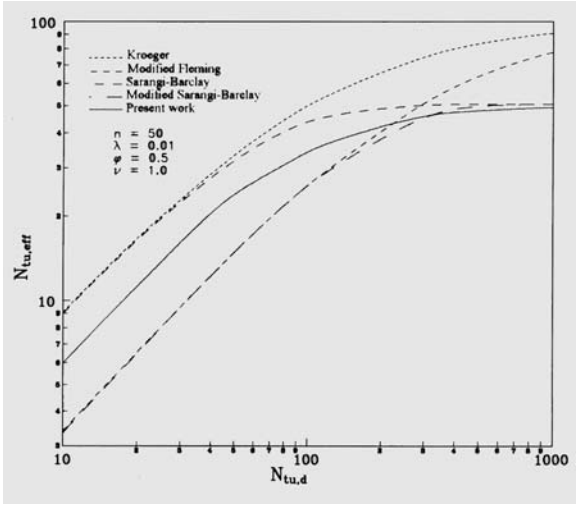

Fig 6. $N_{tu,eff}$ Versus $N_{tu,d}$, for various parameters

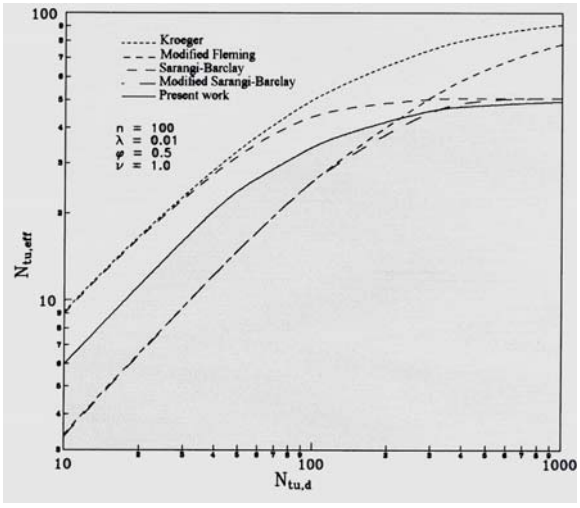

Fig 7. $N_{tu,eff}$ Versus $N_{tu,d}$, for various parameters

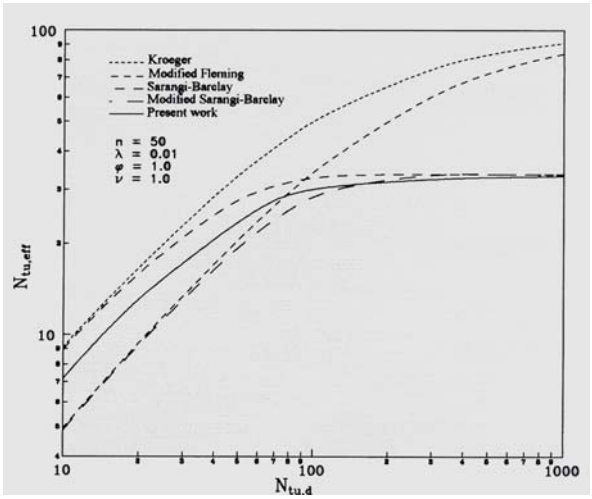

Fig 8. $N_{tu,eff}$ Versus $N_{tu,d}$, for various parameters

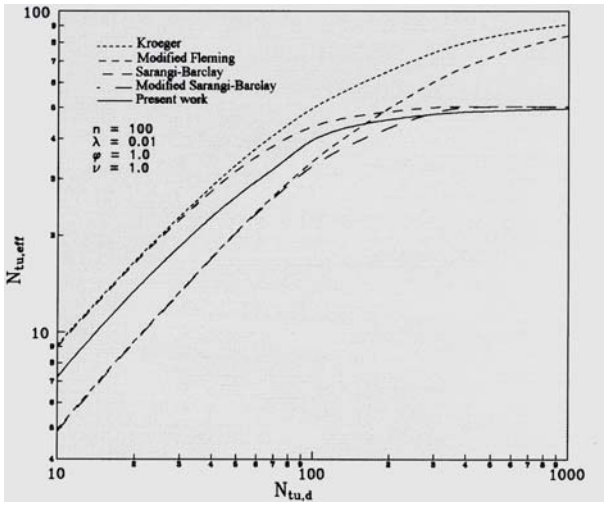

Fig 9. $N_{tu,eff}$ Versus $N_{tu,d}$, for various parameters

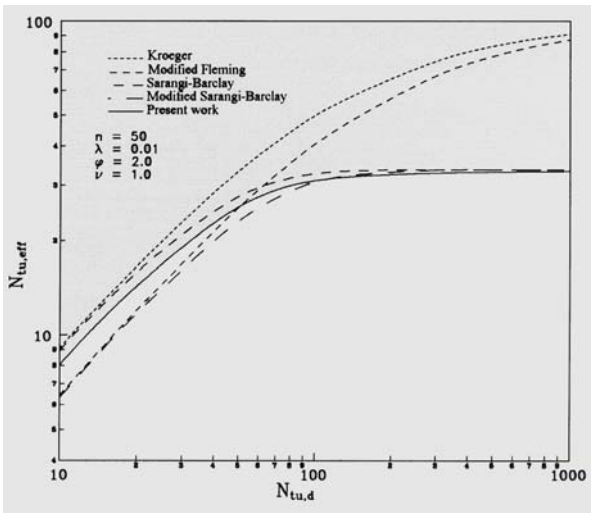

Fig 10. $N_{tu,eff}$ Versus $N_{tu,d}$, for various parameters

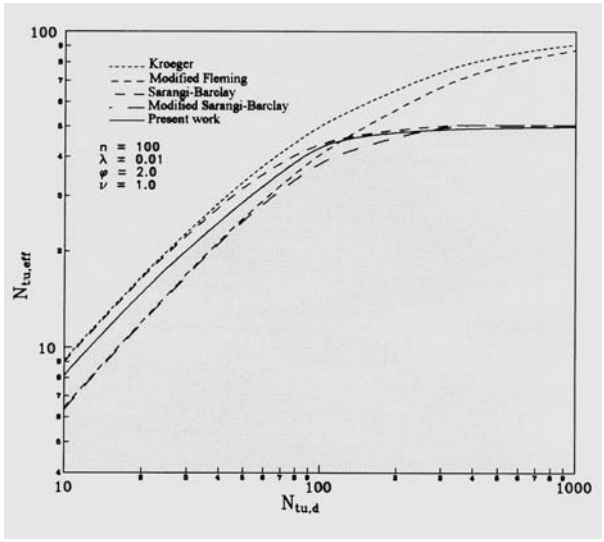

Fig 11. $N_{tu,eff}$ Versus $N_{tu,d}$, for various parameters

Kroeger's formulation considers the effect of axial conduction on the performance of the heat exchanger, but does not consider the effect of plate conduction and the discrete nature of the exchanger. Fleming's approach, on the other hand, accounts for the effect of plate conduction, by considering an equivalent fin efficiency that reduces the effective heat transfer area. However, it ignores axial conduction effects and the discrete nature of the exchanger. We have modified Fleming's model to include the effect of axial conduction, using Kroeger's approach. For the MHE configuration considered, the fin efficiency can be written as [10]:

$$\eta_{fin} = \left[1 + \frac{m_2 {R_2}^2}{8}\right]^{-1} \tag{37}$$

here, $m^2 = hA\dfrac{hA'''}{k_p}$, where h is the heat transfer coefficient, k_p is the effective thermal conductivity of plates in transverse direction, and A''' is the heat transfer area per unit volume of the plate.

Sarangi-Barclay approach considers the effect of finite number of plates and the axial conduction, but it ignores the effect of plate conduction. These effects have been incorporated into the original Sarangi-Barclay formulation by replacing $N_{tu,d}$ with $N_{tu,d} / \lambda_{fin}$. This is the basis of the modified Sarangi-Barclay approach.

At low $N_{tu,d}$, the Kroeger and modified Fleming formulations differ by the fin efficiency factor, while at high $N_{tu,d}$, they approach each other, both being limited by axial conduction effects (see Figs. 7 through 12). The results predicted by the present study, lie between the results of original Sarangi-Barclay and the modified Sarangi-Barclay formulations, the difference being due to the fin efficiency effects. The deviation at low $N_{tu,d}$ is greater for small values of ϕ , as shown in Figs. (7) and

(8). This is because at small $N_{tu,p}$, the plate temperature profile has a larger gradient in the radial direction, which influences the fluid temperature profile. However, at higher $N_{tu,d}$ values the present model and that of Sarangi-Barclay approach each other, and in fact, coincide at sufficiently high values of $N_{tu,d}$.

5. CONCLUSIONS

1. In general, at low $N_{tu,d}$ the effectiveness is fairly independent of n and λ values, and all models give acceptable results. At high $N_{tu,d}$, the effectiveness is limited by n and λ values, instead of $N_{tu,d}$ or ϕ. If $n \prec 1/\lambda$, n is the controlling factor; otherwise $N_{tu,eff}$ is determined by λ.
2. The results of present study lie between those predicted by the original Sarangi-Barclay and the modified Sarangi-Barclay formulations, the difference being due to the fin efficiency effects.
3. The continuum models of Kroeger and Fleming significantly overestimate the effectiveness of the MHE, while those of Sarangi-Barclay and the present numerical model give satisfactory results.

6. REFERENCES

1. Venkatarathnam, G. and Sarangi, S., 1990, "Matrix Heat Exchangers and their Application in Cryogenic Systems", Cryogenics, 30, 907-918.
2. Kirpikov, V.A. and Leifman, I.I., 1972, "Calculation of Temperature Profile of Perforated Fin", Inzhenerno Fizicheskii Zhurnal, 23, 316-321.
3. Venkatarathnam, G., 1991, "Matrix Heat Exchangers", Ph.D. thesis, Indian Institute of Technology, Kharagpur, India.
4. Farhani, F., 1997, "Matrix Heat Exchangers for Cryogenic Applications", Ph.D. thesis, Indian Institute of Technology, Kharagpur, India.
5. Babak, T.B., et. al., 1985, "Applicability of the Convective Heat Transfer Equation for Design of Matrix Heat Exchangers", Theor. Osno. Khim. Tekh Khim., Vol. 19, No.4, 488-494.
6. Sarangi, S. and Barclay, J.A., 1984, "An Analysis of Compact Heat Exchanger Performance", In *ASME, Cryogenic Process and Equipment*-1984, pp. 37-44, New Orleans, Louisiana.
7. Kroeger, P.G., 1967, "Performance Determination of High Performance Heat Exchangers, due to Axial Heat Conduction Effects", Advances in Cryogenic Engineering, 12, 363-372.
8. Von Rosenberg, D.U., 1969, *Methods for the Numerical Solution of Partial Differential Equations*, American Elsevier Publishing Company, New York.
9. Fleming, R.B., "A Compact perforated plate Heat Exchanger", Advances in Cryogenic Engineering, 14, 197-204.
10. Rodriguez, J.I., 1991, "Heat Transfer and Flow Friction Characteristics of Perforated Plate Heat Exchangers", Ph.D. thesis, Mechanical Engineering Department, University of California, Los Angeles, USA.

7. MAILING ADDRESS

Dr. F. Farhani
Mechanical Engineering Department,
I.R.O.S.T., P.O. Box 15815 – 3538, Tehran, Iran
Phone: (009821)88838345
Fax: (009821)88838345
E-mail: ffarhani@yahoo.com